Supporting information

Synthesis and Characterisation of λ-Carrageenan Oligosaccharide-Based Nanoparticles: Applications in MRI and *in vivo* Biodistribution Studies

M. Porta Zapata, S. Carregal-Romero, J. Saliba, L. Martínez-Parra, A. Urkola-Arsuaga, C.B. Miranda Perez de Alejo, I. Orue, D. Di Silvio, A. Descamps-Mandine, C. Daviaud, M. Menard, B. Musnier, J. Cherfan, A. Codault, C. Manseur, M. Jeannin, D. Castejon, I. Fruitier-Arnaudin, J. Ruiz-Cabello, H. Groult

1) Characterization of the λ-COS NP structure

2) Magnetic properties assessment of the λ-COS NP

3) *In vivo* experiments

4) *Ex vivo* experiments

1) Characterization of the λ-COS NP structure

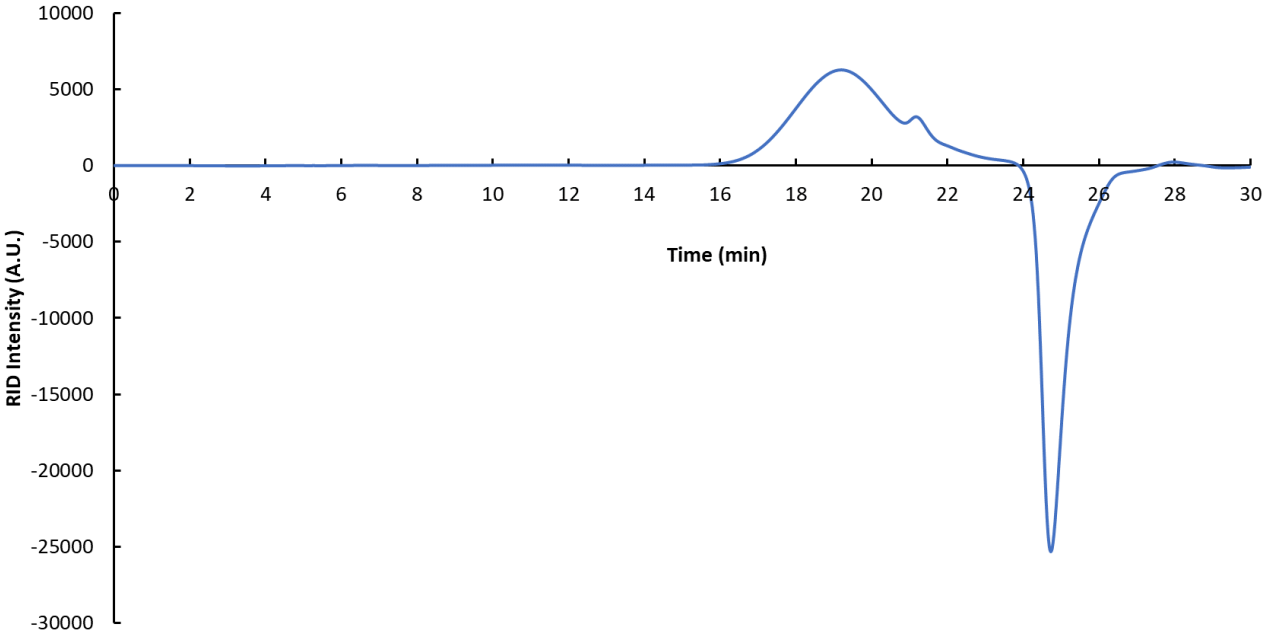

Figure S1: SEC-HPLC spectra of λ-COS

The molecular weight of the λ-COS was measured using an Agilent 1260 Infinity II system, composed of two analytical columns (TSK-GEL G4000PW and TSK-GEL G3000PWXL) coupled with a Refractive Index Detector (RID). MW was calibrated using heparin standards (from 1200 to 5200 Da).

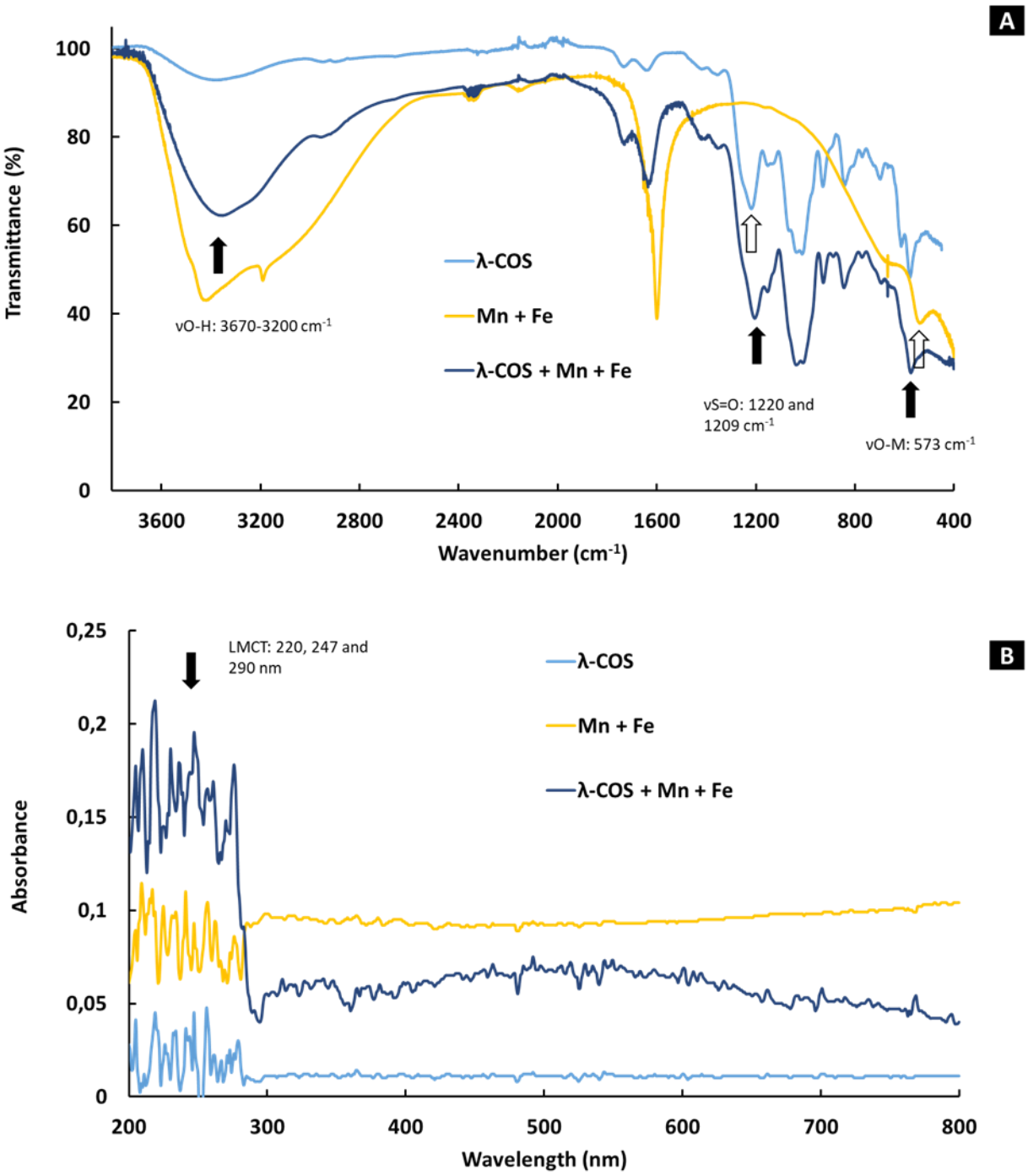

Figure S2: (A) FT-IR and (B) UV-visible spectra of water soluble metals- λ-COS coordination complex

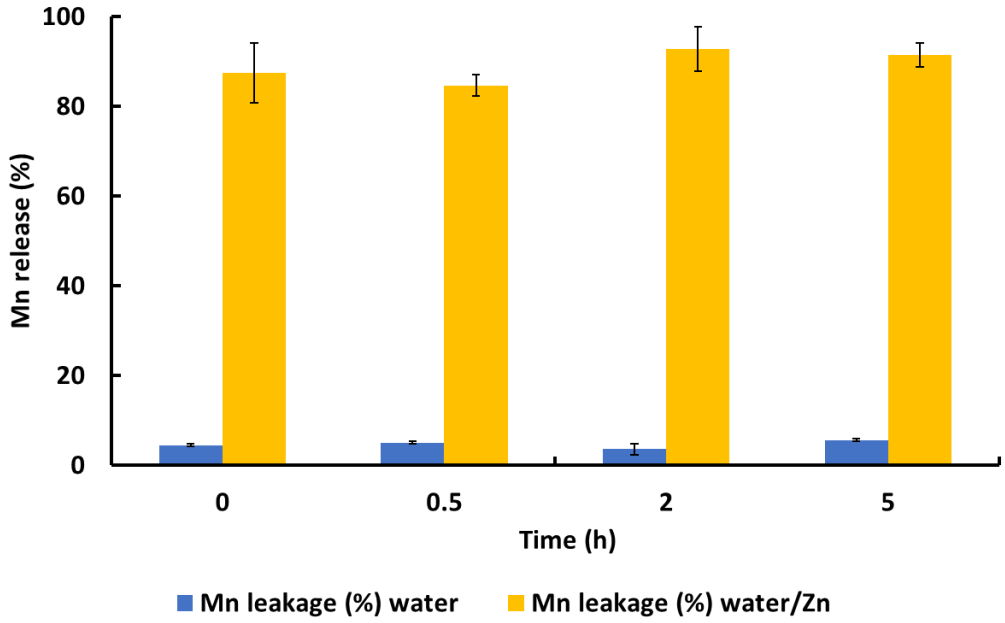

Figure S3: Mn released assessment

Several microscopic images were realized to help characterize the structure of the λ-COS NP. ***Figure S4A*** shows the image used to measure the average size of the cores (2.6 ± 0.4 nm, N=250) using the software Imagej®. ***Figures S4B*** **and** ***S4C*** were done by high-resolution TEM in bright-field mode and dark field mode, respectively. ***Figure S4B*** was used to determine the d-scaping using the FFT functionality of the software Imagej®.The diffraction pattern obtained from this image is presented in ***Figure S7*** and miller index identified were attributed according to literature as manganese ferrite.[3] High resolution TEM associated with EDS was also used to determine the atomic arrangement within the sample: ***Figure S5*** with a map and ***Figure S6*** with a line analysis. Finally, XPS characterisation of the λ-COS coating in free form or nano-formulated is displayed in ***Figure S9***.

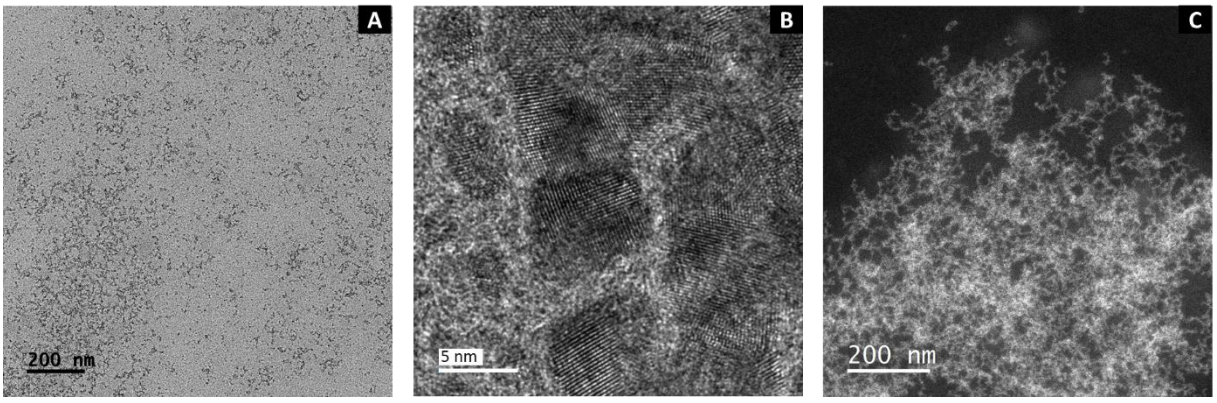

Figure S4: TEM and HRTEM images of the λ-COS NP in bright field (A and B) and dark field (C).

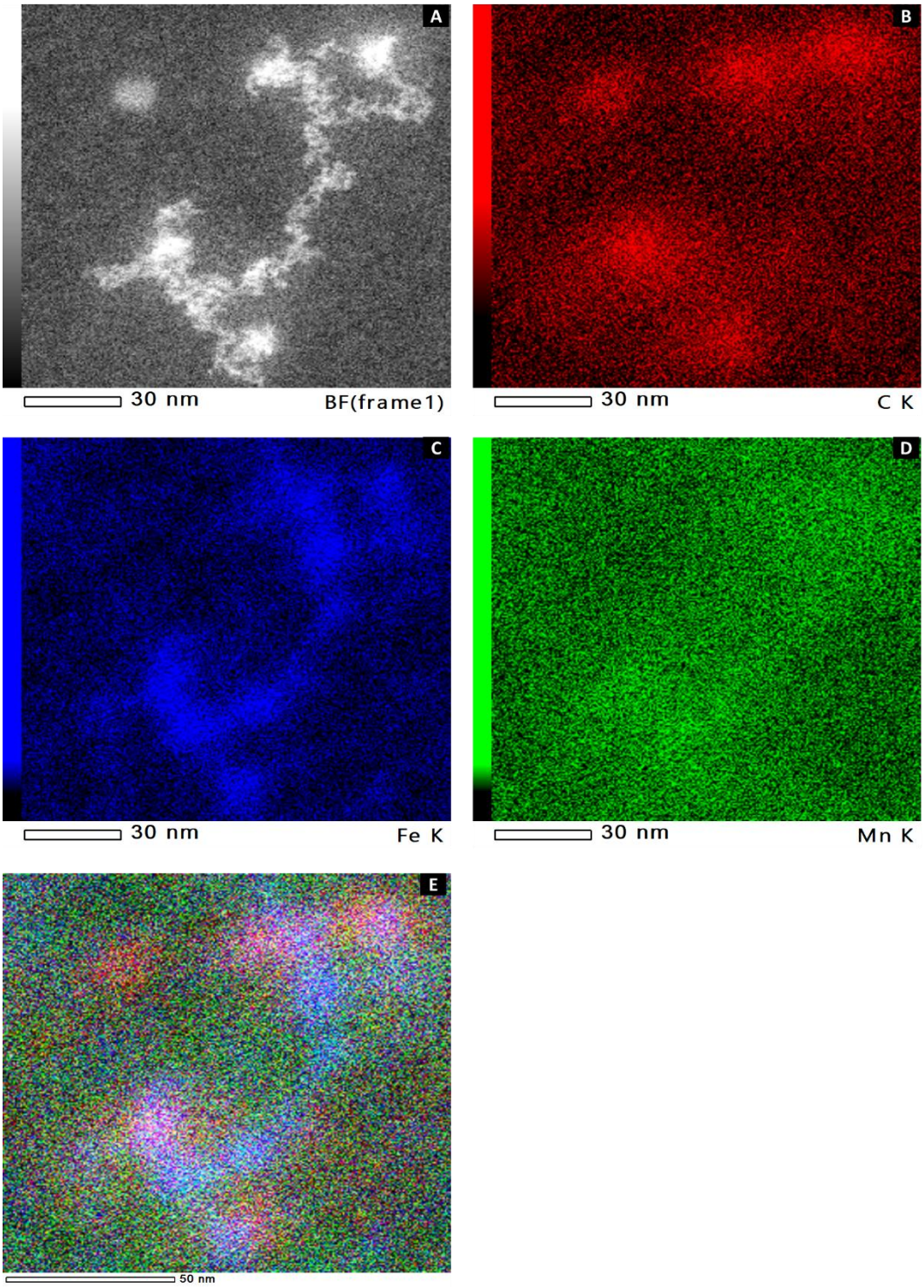

Figure S5: HRTEM images (A) associated with EDS in maps: (B) Carbon, (C) Iron, (D) Manganese, (E) Merge map.

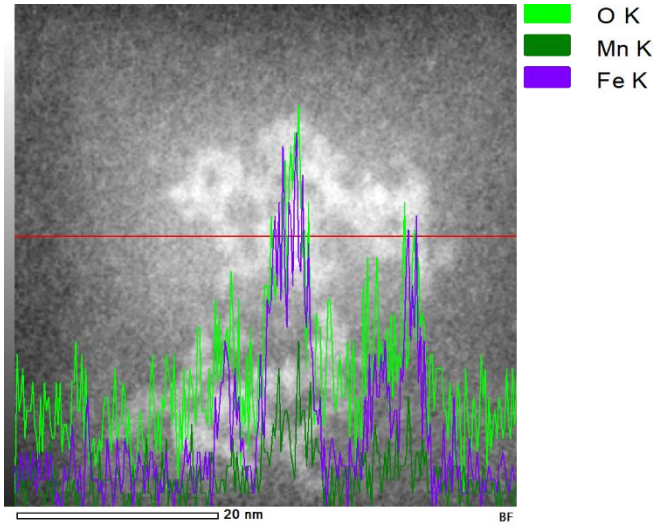

Figure S6: HRTEM images associated with EDS in line.

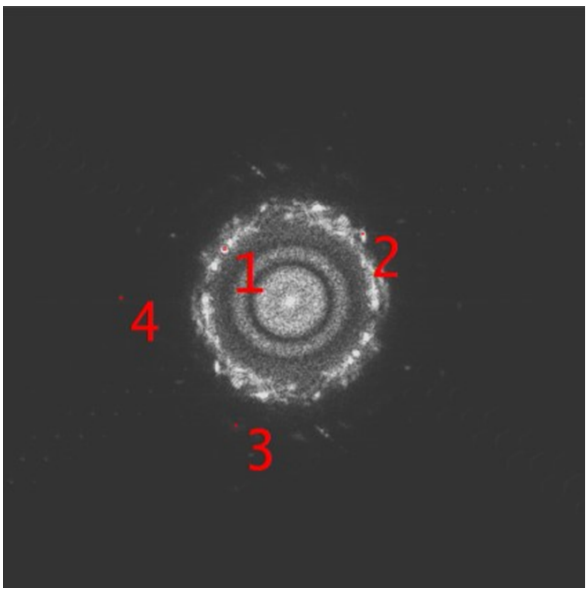

Spot#	d-Spacing (Å)	Miller index (hkl)
1	2.383	220
2	2.139	311
3	1.460	400
4	1.174	331

Figure S7: Diffraction pattern and d-spacing.

Mw λ-COS (kDa)	**Average core diameter of the encapsulated ferrites (nm)**	**Average volume of one ferrite core (nm3)** *considering a sphere*	**Average surface of one ferrite core (nm2)** *considering a sphere*	**Average volume of one ferrite core (cm3)** *considering a sphere*
7,2	2,6	9,2	21,2	9,2E-21
Average weight of one ferrite core (mg)	**Average Fe weight in one ferrite core (mg)**	**Average Mn weight in one ferrite core (mg)**	**Average O weight in one ferrite core (mg)**	**[λ-COS] mg/mL**
4,8E-17	3,2E-17	1,5E-18	1,3E-17	10,4
[Fe] total (mg/mL)	**[Mn] total (mg/mL)**	**[Mn] included in ferrite cores (mg/mL)**	**[Mn] Free complexed in the NP (mg/mL)**	**Number NP /ml measured by MALS**
0,57	0,37	0,04	0,33	6,46E+11
Estimated number of ferrite cores /ml *based upon iron concentration*	**Estimated number of ferrite cores in one λ-COS NP**	**Estimated number of complexed Mn /ml**	**Estimated number of free Mn in one λ-COS NP**	
1,75E+16	2,71E+04	3,66E+18	5,67E+06	
Estimated number of λ-COS /ml	**Estimated number of λ-COS in one λ-COS NP**	**Estimated number of complexed Mn per λ-COS chain**	**Estimating apparent number of λ-COS chains per ferrite core**	**Estimating apparent grafting density** *(number of λ-COS chains/nm²)*
8,70E+17	1,35E+06	4,2	49,7	2,34

Table S8: Calculation of different key parameters related to the structure of the λ-COS NP.

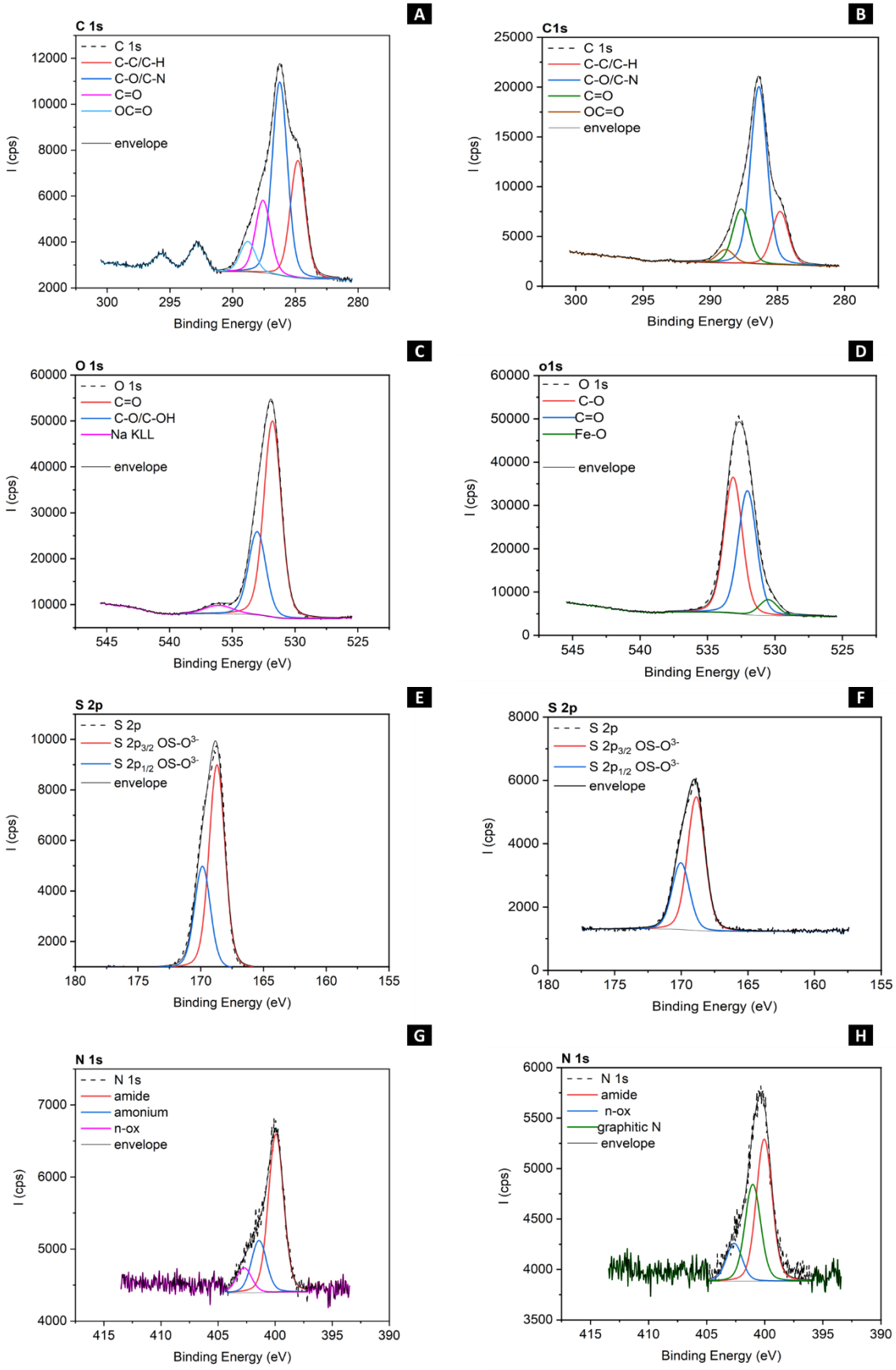

Figure S9: XPS coating characterization: (A-B) C 1s, (C-D) O 1s, (E-F) S 2p, (G-H) N 1s signals, left-hand column (A,C,E,G) correspond to λ-COS and right-hand column (B,D,F,H) to λ-COS NP.

2) Magnetic properties assessment

To go further in the magnetic properties assessment of the λ-COS NP, the magnetic moment was measured at different temperatures, from 2k to 300K (***Figure S10***).

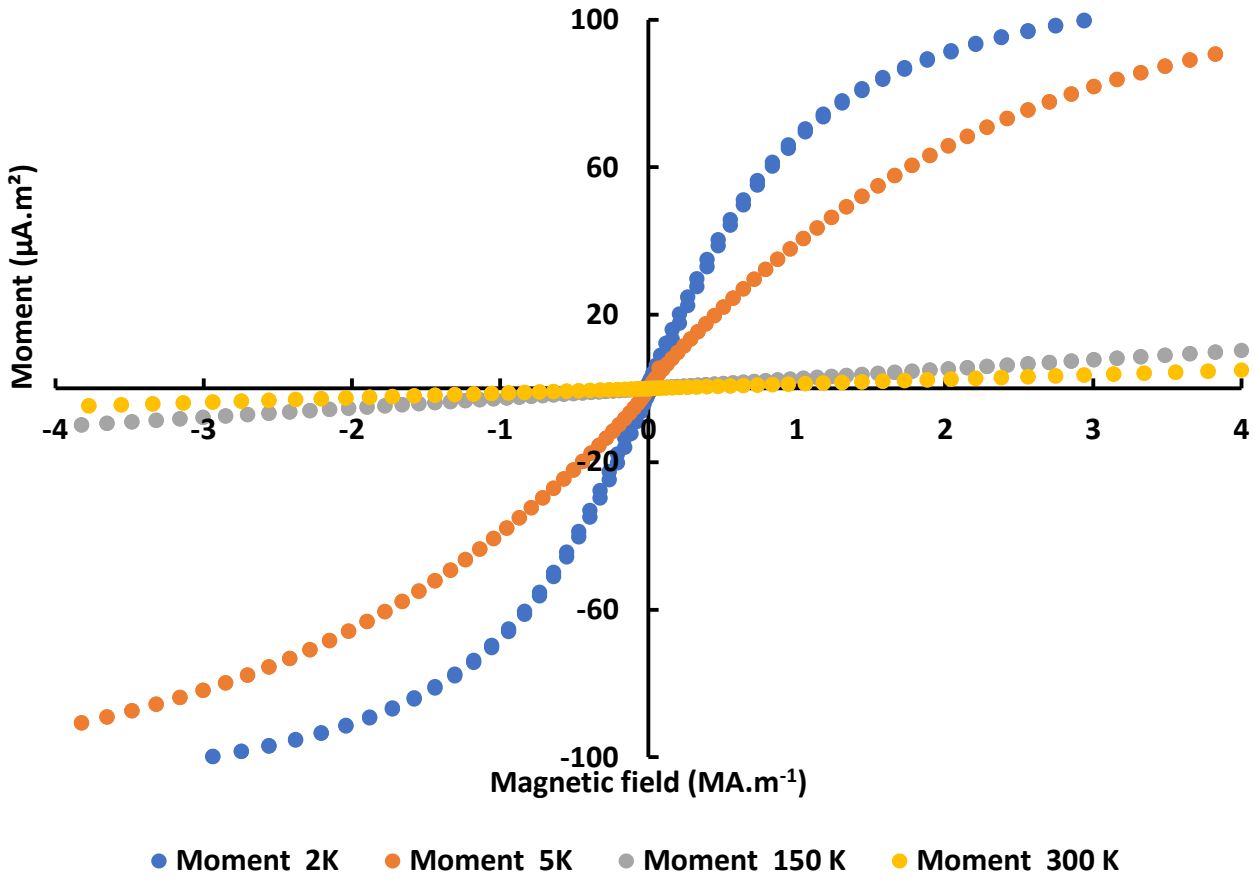

Figure S10: Magnetic moment at different temperatures.

Prior to *in vivo* experiments, the ability of the λ-COS NP to produce a contrast in MRI was assessed by realisation of phantoms. Several solutions of λ-COS NP were realised with a gradient of concentration in Fe + Mn and T_1 and T_2 maps were measured using MRI at high field (7T) in ***Figure S11A*** and at low-middle field (1T) in ***Figure S11B***. The r_1 was slightly affected by the change of magnetic field, its values stayed around 2 $mM^{-1}{\cdot}s^{-1}$. However, for the r_2, a significant rise was measured at 7T with a value of 52.7 $mM^{-1}{\cdot}s^{-1}$ compared to the value obtained by the 1T MRI at 14.6 $mM^{-1}{\cdot}s^{-1}$.

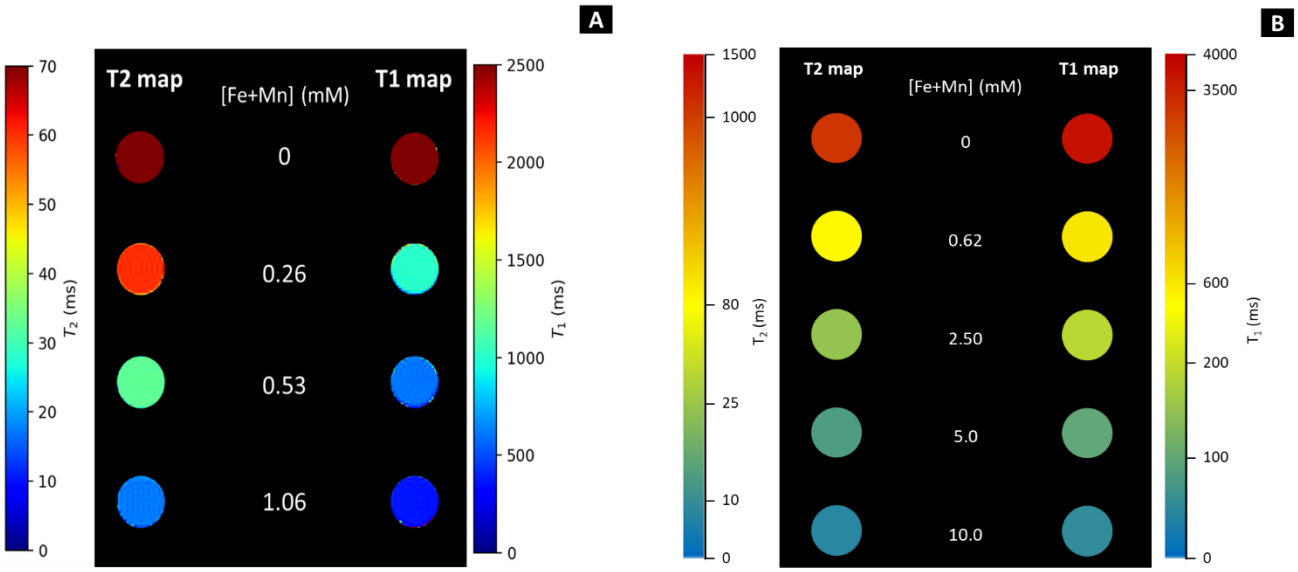

[Fe+Mn] (mM)	T1 (ms)	T2 (ms)	1/T1 (s^{-1})	1/T2 (s^{-1})
0	3689.2	504.2	0.3	2.0
0.26	998	60	1.0	16.7
0.53	602	32.7	1.7	30.6
1.06	366.2	17.3	2.7	57.8

r1 ($mM^{-1}.s^{-1}$)	r2 ($mM^{-1}.s^{-1}$)	r2/r1
2.3	52.7	22.9

[Fe+Mn] (mM)	T1 (ms)	T2 (ms)	1/T1 (s^{-1})	1/T2 (s^{-1})
0	3750	1199	0.27	0.83
0.6	620	77	1.6	12.9
2.5	183	24	5.5	41.6
5.0	96	12.8	10.4	78
10.0	51	6.7	19.7	148

r1 ($mM^{-1}.s^{-1}$)	r2 ($mM^{-1}.s^{-1}$)	r2/r1
1.9	14.6	7.5

Figure S11: Phantoms: (A) at 7T and at 37°C and (B) at 1T and at 37 °C.

3) *In vivo* experiments

Table S12: Table listing the in vivo experiments.

All *in vivo* experiments and *ex vivo* analyses that were realised are indexed in ***Table S12***.

General parameters				MRI			ICP-MS		Histology	
Nbr mice total	Injected volume (µL)	[Mn] injected ($\mu M \cdot kg^{-1}$) *	[Fe+Mn] ($mg \cdot mL^{-1}$)	Nbr mice MRI	Type of MRI	Type of MRI XP	Nbr Mice ICP-MS	Type of ICP-MS	Nbr of mice histo	Type of histo
2	50	11.8	0.8	2	7T	basal, 2h and 24h	2	at 24h at 24h	0	X
4	50	21.8	1.3	2	7T	basal, 1h and 24h	3	at 24h at 24h at 24h	0	X
				X				Urine		
4	70	32.8	1.5	2	7T	basal, 30 min and 24h	2	at 24h at 24h	2	at 24h Control
8	70	32.8	1.5	0	X		5	at 24h at 3h at 3h Control at 24h	3	at 3h at 3h Control
									X	
5	50	23.9	1.6	5	1T	Monitoring until 3h30 Monitoring until 2h Monitoring until 2h Monitoring until 3h Monitoring until 4h	0	X	0	X
3	100	47.8	1.6	3	1T	Monitoring until 4h30 after injection and image 24h Monitoring until 6h and image at 24h	0	X	0	X
1	100	95.5	3	1	1T	Monitoring until 4h30 after injection and image 24h	0	X	0	X

** Average mouse weight considered: 20 g*

Several sequences in MRI were conducted to follow the biodistribution of the λ-COS NP. ***Figures S13, S14*** and ***S15*** were realized at low field (1T) using, respectively, a T_1-weighted gradient echo sequence, T_2-weighted gradient echo sequence and a Multi-Spin Multi-Echo (MSME) sequence. ***Figure S16*** displays a comparison of contrast performance between λ-COS NP and Multihance® with T_1-GE sequence. ***Figure S17*** represents the biodistribution of the λ-COS NP monitored at high field (7T) with a T_2 relaxometric map constructed from a MSME sequence and a GE-Flash sequence, and ***Figure S18*** represents the corresponding quantification of T_2 values in the main organs.

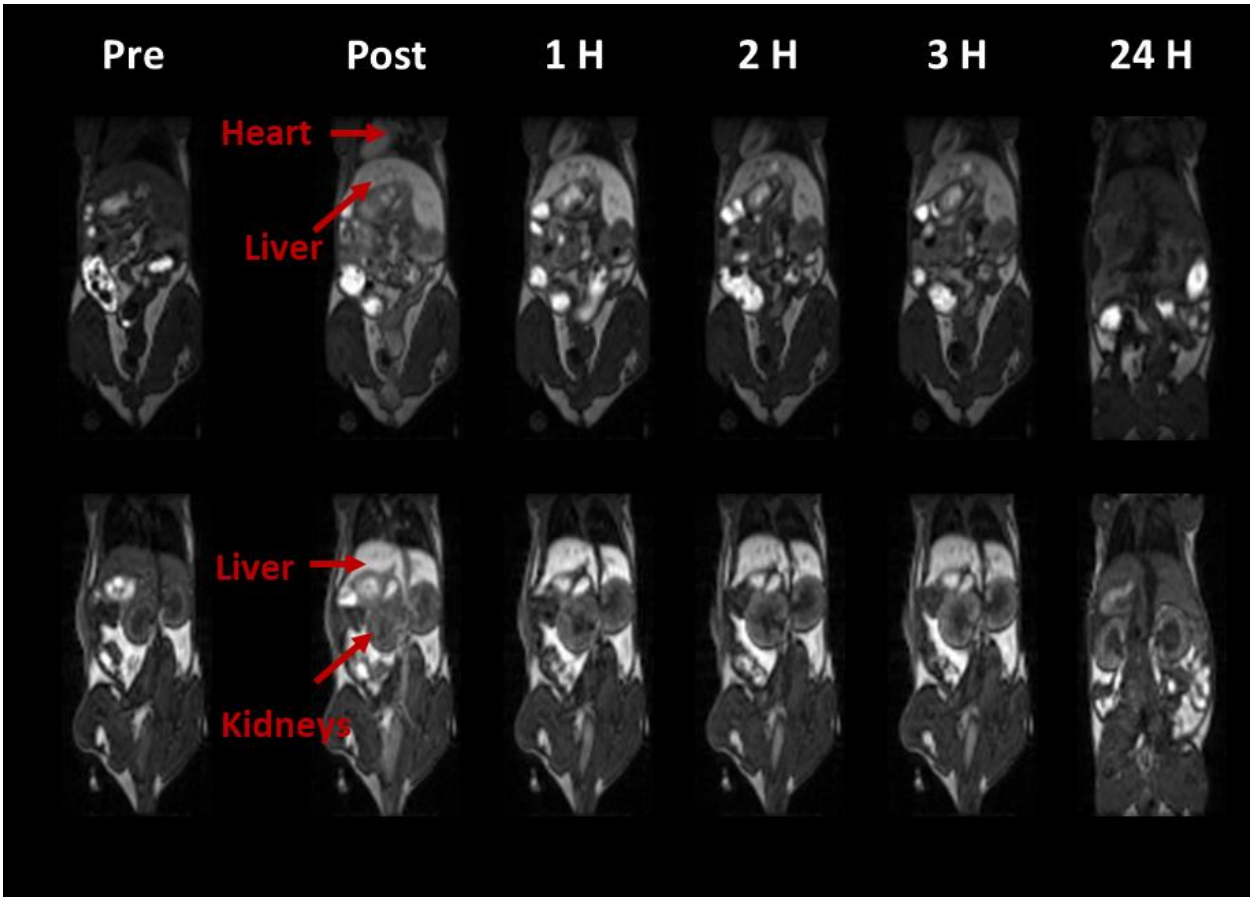

Figure S13: Biodistribution study in MRI at low field (1T) with a T_1-weighted gradient echo sequence of a second representative case. Coronal views of the upper and the abdominal regions brightening the heart, liver, intestine and kidneys. I.v. administration of 100 µL λ-COS NP solution at [Fe + Mn] = 1.6 mg·mL $^{-1}$.

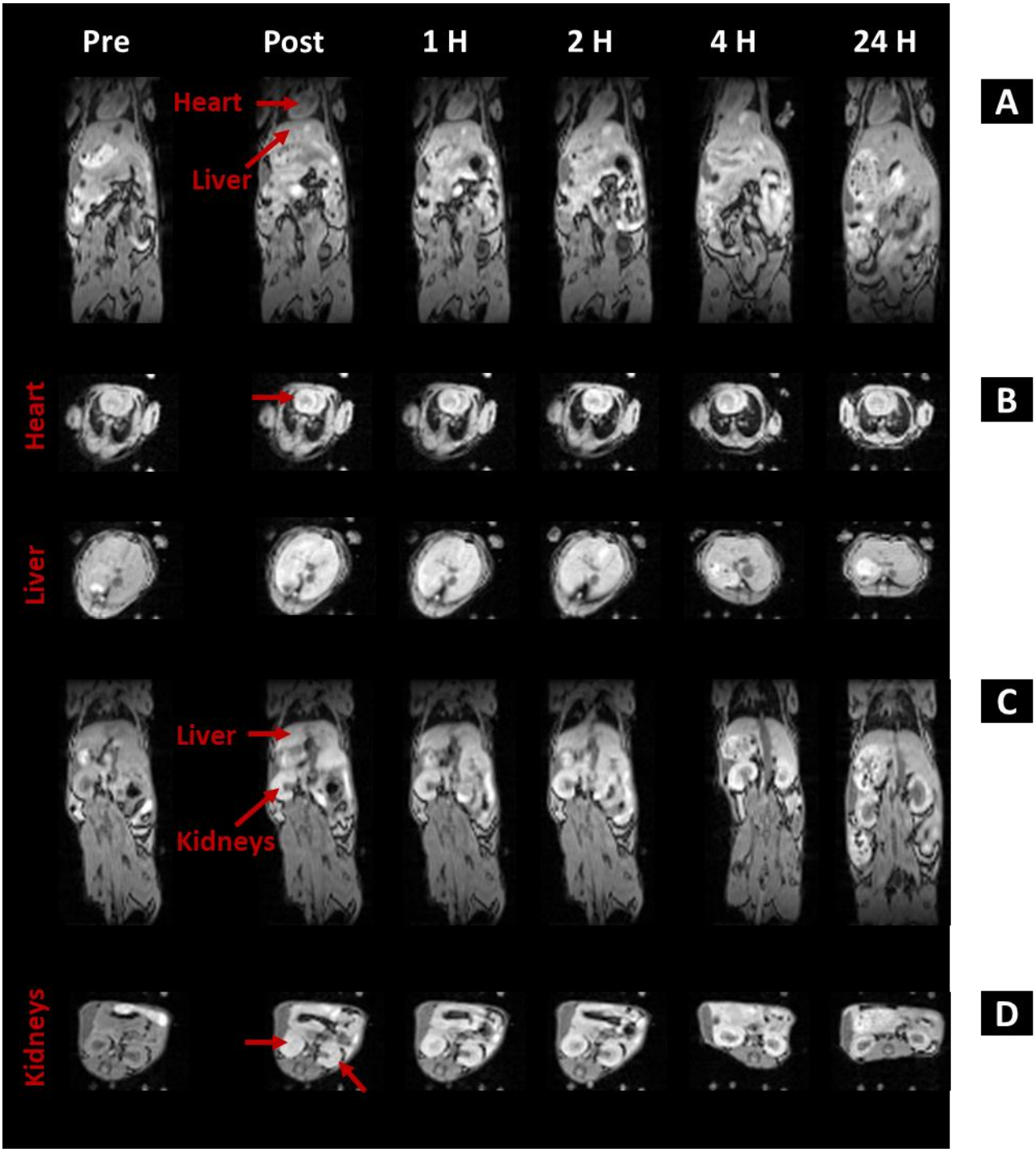

Figure S14: Biodistribution study in MRI at low field (1T) with a T_2-weighted gradient echo sequence of one representative case. Coronal views of the upper abdominal region (A) and axial views of the heart and liver (B), additional coronal views of the lower abdominal region (C) and axial views of the kidneys (D). I.v. administration of 100 µL λ-COS NP solution at [Fe + Mn] = 3 mg·mL^{-1}.

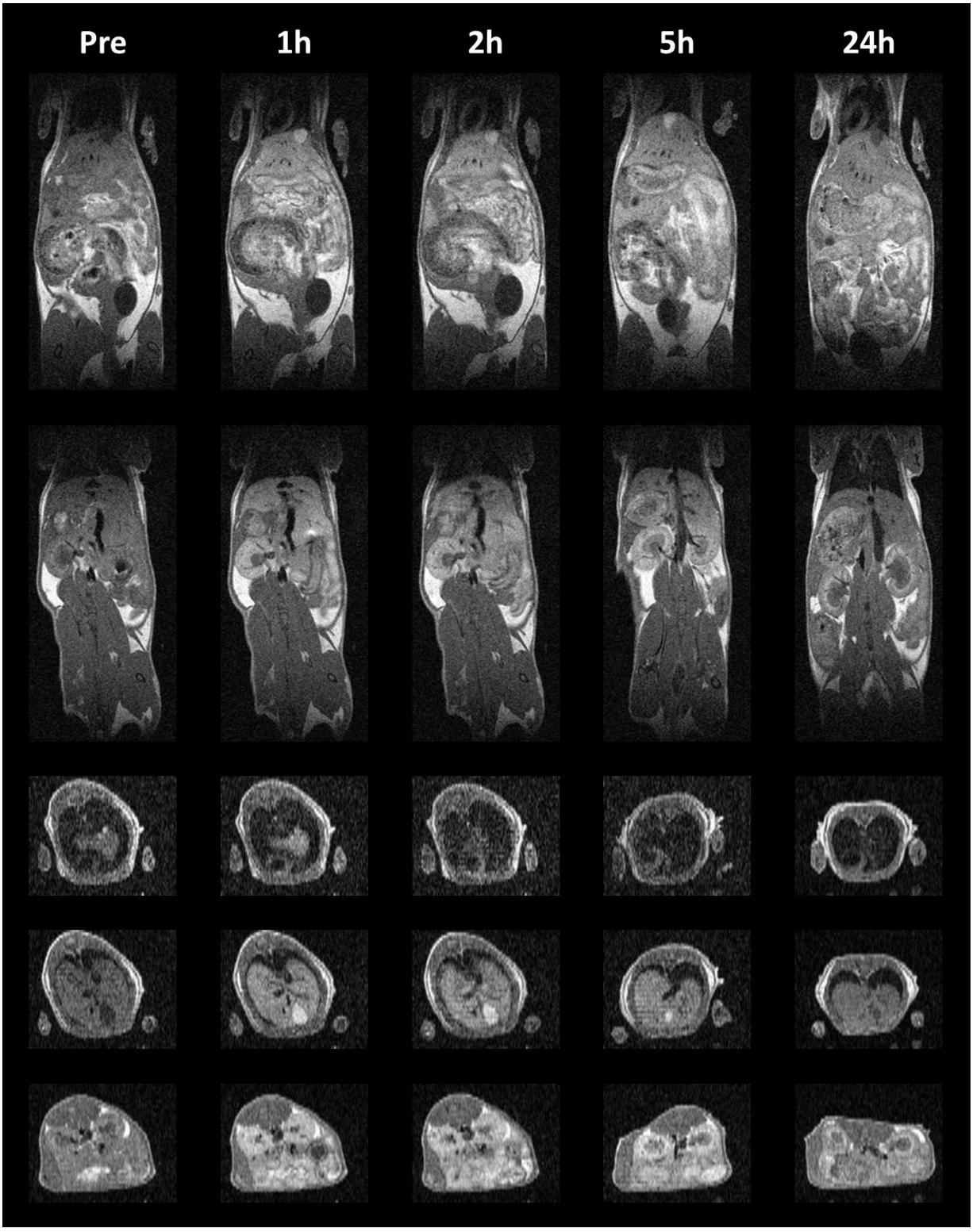

Figure S15: MRI (1T) images (MSME sequency). I.v. administration of 100 µL λ-COS NP solution at [Fe + Mn] = 3 mg·mL $^{-1}$.

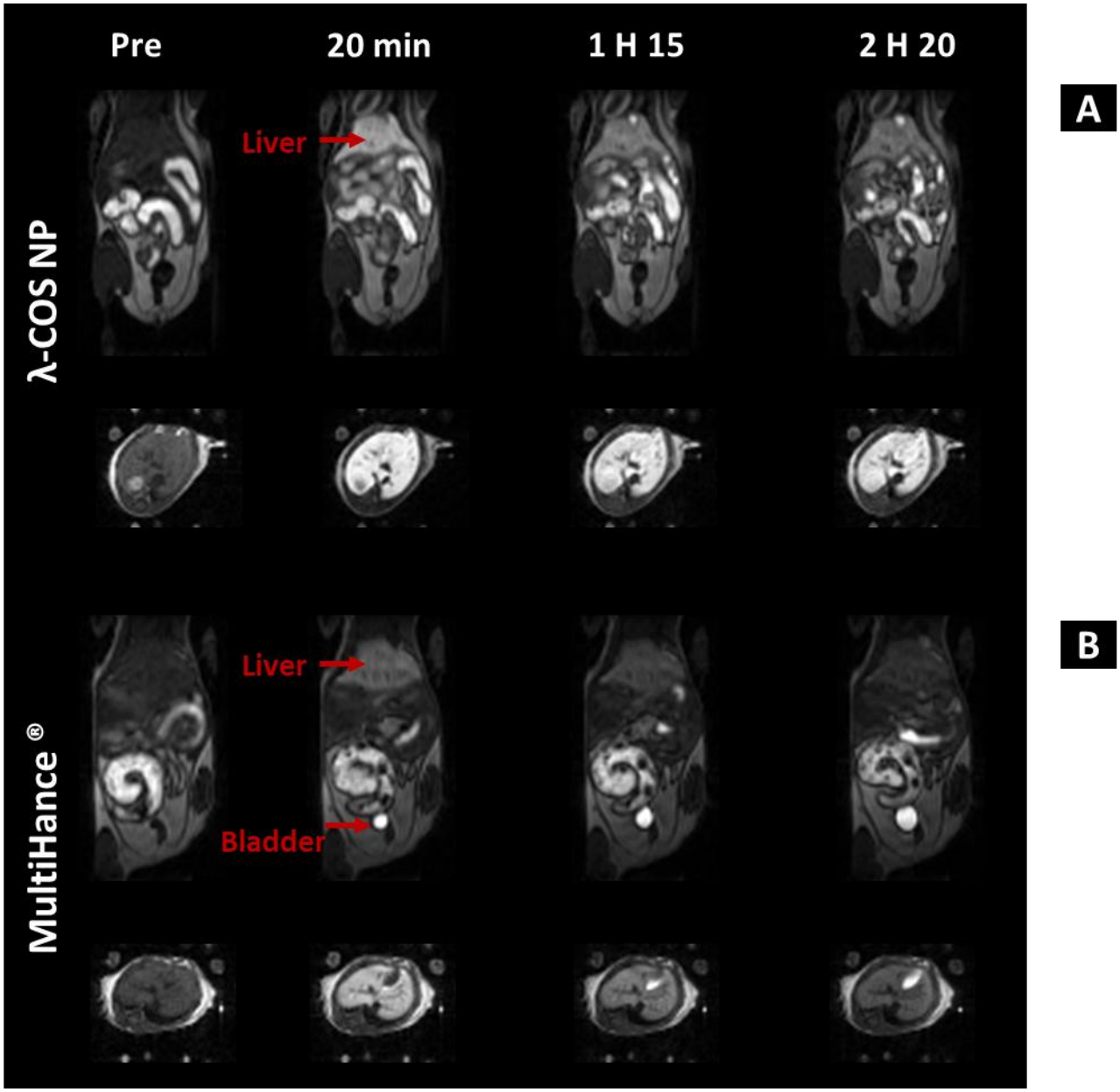

Figure S16: Comparison of contrast performance between (A) λ-COS NP with an injected Mn dose of ~24 µM·kg^{-1} and (B) Multihance® with an injected Gd doses of ~116 µM·kg^{-1}. Upper images are coronal views brightening heart, liver and bladder, while lower images are axial views of the liver. I.v. administration of 50 µL of CA solution at [Fe + Mn] = 1.6 mg·mL^{-1}.

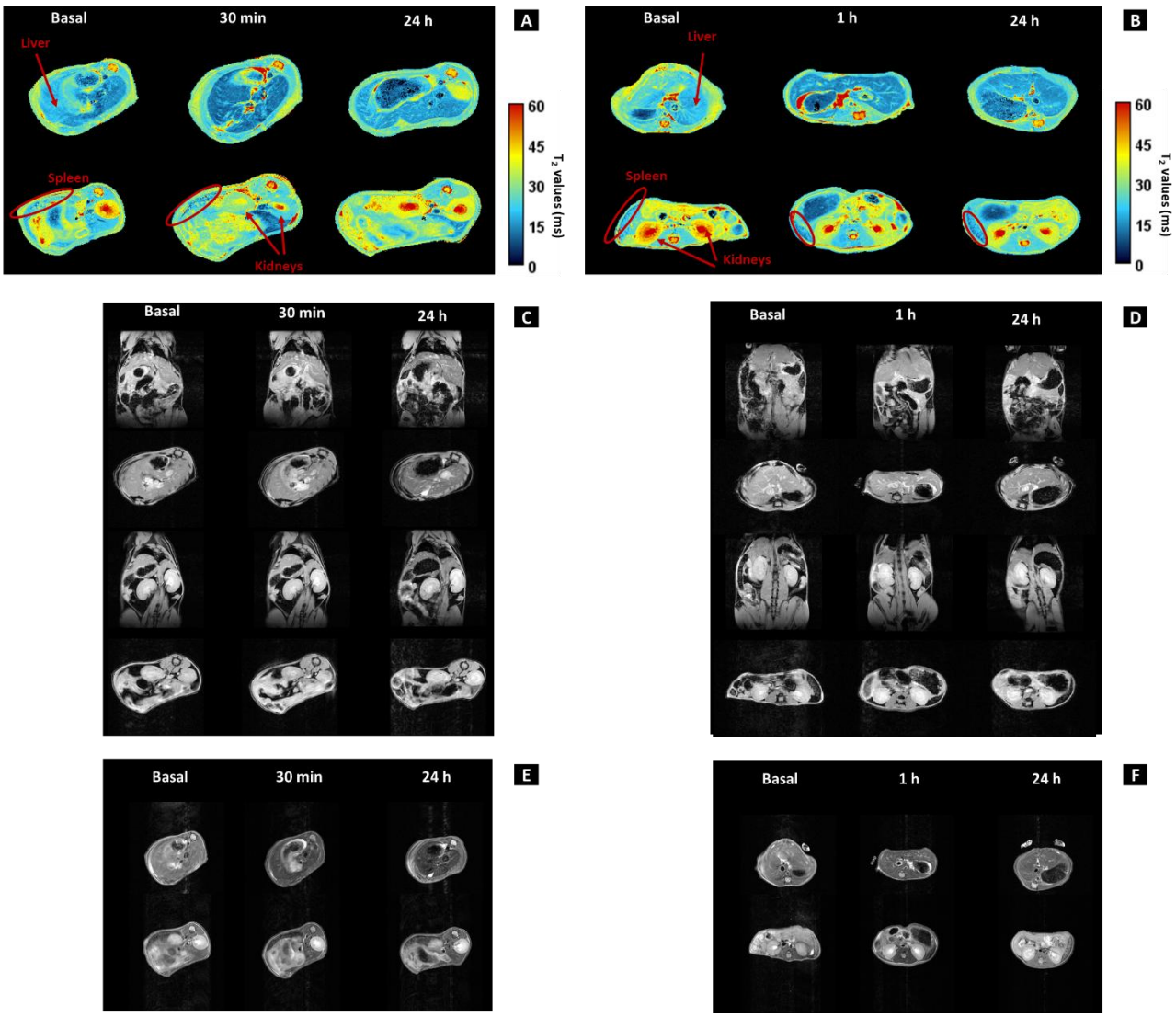

Figure S17: Two biodistribution studies in MRI at high field (7T) with (A, B) a T_2 relaxometric map constructed from a MSME sequence (two axial views of the liver and kidneys) ; (C, D) a GE-Flash sequence (TE=4 ms, TR=600 ms, FA 30°), two coronal views (line 1 and 3) and axial views (line 2 and 4) showing mainly the liver and kidneys are included ; (E, F) Typical axial images of liver and kidneys obtained in one MSME step (TE=16 ms, TR=4000 ms, FA 90°). I.v. injection of 70 µL λ-COS NP solution at [Fe + Mn] = 1.5 mg·mL^{-1} for left-hand case (A, C and F images) and 50 µL λ-COS NP solution at [Fe + Mn] = 1.3 mg·mL^{-1} for right-hand case (B, D and E images)

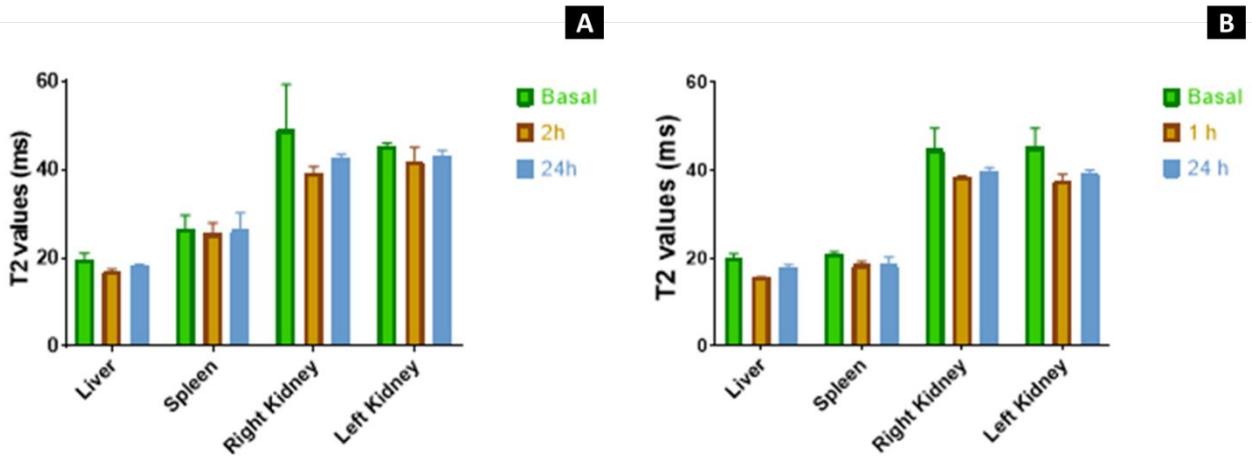

Figure S18: T_2-value quantification in selected ROI of different organs, pooling together the contrast points of two mice with (A) an injected volume of 50 µL of λ-COS NP solution, [Fe + Mn] = 0.8 mg·mL^{-1}, and (B) an injected volume of 50 µL [Fe + Mn] = 1.3 mg·mL^{-1}.

4) *Ex vivo* experiments

Histopathology of tissues 24 h after the injection of the λ-COS NP was realised using H.E. and P.B. staining. Prussian blue staining was also used to highlight the presence of iron within the tissue. Blue dots corresponding to NP's iron detectable in comparison to the control tissues, as indicated by arrows. It can be found in the lungs, liver and spleen tissues.

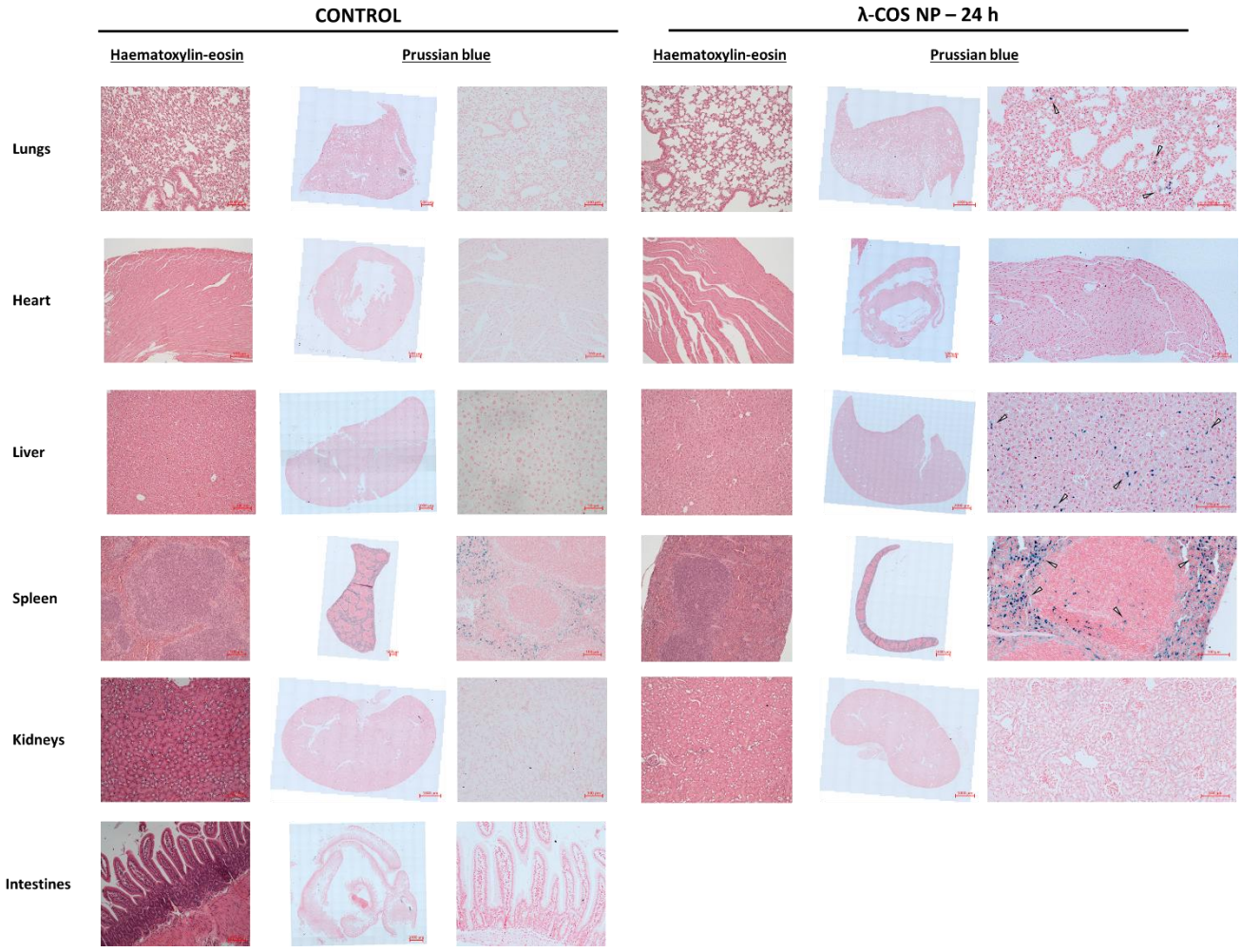

Figure S19: Histopathology, 24 h after the injection (A) stained in H.E., (B) stained in P.B. Injected volume: 70 µL with [Fe + Mn] = 1.5 mg·mL^{-1}, n = 1. On PB images, arrows indicate the blue stains corresponding to NP's iron detectable.

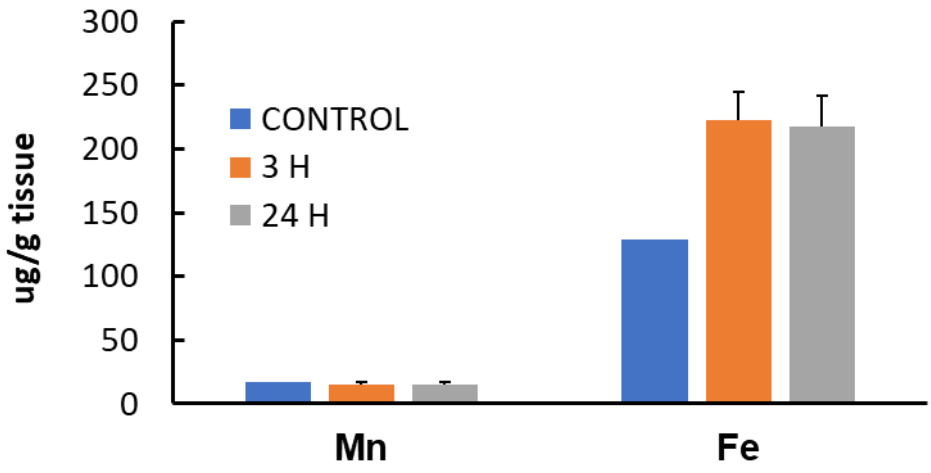

Figure S20: Mn and Fe content in intestine measured by ICP-MS and expressed in mass (µg) of metallic ions per g of dry tissue. Injected volume: 70 µL with [Fe + Mn] = 1.5 mg·mL^{-1}, the data are mean ± SEM of n=2 mice.

Supporting Information bibliography

(1) Groult, H.; Carregal-Romero, S.; Castejón, D.; Azkargorta, M.; Miguel-Coello, A.-B.; Reddy Pulagam, K.; Gómez-Vallejo, V.; Cousin, R.; Muñoz-Caffarel, M.; H. Lawrie, C.; Llop, J.; Piot, J.-M.; Elortza, F.; Maugard, T.; Ruiz-Cabello, J.; Fruitier-Arnaudin, I. Heparin Length in the Coating of Extremely Small Iron Oxide Nanoparticles Regulates in Vivo Theranostic Applications. *Nanoscale* **2021**, *13* (2), 842–861. https://doi.org/10.1039/D0NR06378A.

(2) Groult, H.; Poupard, N.; Herranz, F.; Conforto, E.; Bridiau, N.; Sannier, F.; Bordenave, S.; Piot, J.-M.; Ruiz-Cabello, J.; Fruitier-Arnaudin, I.; Maugard, T. Family of Bioactive Heparin-Coated Iron Oxide Nanoparticles with Positive Contrast in Magnetic Resonance Imaging for Specific Biomedical Applications. *Biomacromolecules* **2017**, *18* (10), 3156–3167. https://doi.org/10.1021/acs.biomac.7b00797.

(3) Diodati, S.; Pandolfo, L.; Caneschi, A.; Gialanella, S.; Gross, S. Green and Low Temperature Synthesis of Nanocrystalline Transition Metal Ferrites by Simple Wet Chemistry Routes. *Nano Res.* **2014**, *7* (7), 1027–1042. https://doi.org/10.1007/s12274-014-0466-3.